Langmuir
Article
pubs.acs.org/Langmuir

Controlling the Morphology of Photosystem I Assembly on Thiol-Activated Au Substrates

Dibyendu Mukherjee,[†,‡] Mark May,[†,‡] Michael Vaughn,[†,§,∥] Barry D. Bruce,[†,‡,§] and Bamin Khomami*[,†,‡]

[†]*Sustainable Energy Education and Research Center (SEERC),* [‡]*Department of Chemical and Biomolecular Engineering,* [§]*Department of Biochemistry, Cellular and Molecular Biology, University of Tennessee, Knoxville, Tennessee 37996.* [∥]*Current address: Department of Chemistry and Biochemistry, Arizona State University, Tempe, AZ 85287.*

Received July 15, 2010. Revised Manuscript Received August 17, 2010

Morphological variations of Photosystem I (PS I) assembly on hydroxyl-terminated alkanethiolate self-assembled monolayer (SAM)/Au substrates with various deposition techniques is presented. Our studies indicate that deposition conditions such as PS I concentration and driving force play a central role in determining organization of immobilized PS I on thiol-activated Au surfaces. Specifically, atomic force microscopy (AFM) and ellipsometry analyses indicate that gravity-driven deposition from concentrated PS I solutions results in a large number of columnar PS I aggregates, which assemble perpendicular to the Au surface. PS I deposition yields much more uniform layers when deposited at lower concentrations, suggesting preassembly of the aggregate formation in the solution phase. Moreover, in electric-field assisted deposition at high field strengths, columnar self-assembly is largely prevented, thereby allowing a uniform, monolayer-like deposition even at very high PS I concentrations. In situ dynamic light scattering (DLS) studies of solution-phase aggregation dynamics of PS I suspensions in both the presence and absence of an applied electric field support these observations and clearly demonstrate that the externally imposed electric field effectively fragments large PS I aggregates in the solution phase, thereby permitting a uniform deposition of PS I trimers on SAM/Au substrates.

Introduction

In nature, plants and algae have evolved an advanced photosynthesis mechanism that harnesses solar energy in a highly efficient manner with nearly 100% quantum efficiency. Photosystem I (PS I) is a supramolecular protein complex[1] which functions as a biological photodiode[2] and undergoes photochemical charge separation resulting in unidirectional electron transfer between the reaction center (P700) electron donor on the lumenal side and Fe−S clusters (F_A, F_B, F_X)[3] at the stromal side. For PS I isolated from the thermophilic cyanobacteria, *Thermosynechococcus elongatus* (TE), the structural and dimensional characteristics of PS I are well-documented[4] (see Figure 1 for details). These structural properties combined with the strong electrochemical properties makes PS I an ideal candidate for incorporation into solid-state bioelectronic or hybrid photovoltaic devices.[5−8] However, rational design and optimization of these devices require clear elucidation of the surface attachment dynamics and properties of these protein complexes on various substrates.

Gravity-driven sedimentation of detergent-solubilized PS I onto alkanethiolate self-assembled monolayer (SAM)/Au surfaces[9,10] has received attention in recent years. More recently, assisted deposition techniques including attachment of PS I layers on Au electrodes using solvent evaporation under vacuum[11] has been explored. The main limiting step in converting these relatively simple, lab-based concepts into practical, optimized devices lies in the difficulty of producing a uniform and densely packed PS I monolayer on organic/inorganic interfaces. Earlier studies have suggested that PS I attaches favorably onto OH-terminated thiols without denaturation[9−11] and with ∼70% of the electron-transfer vectors pointing outward.[12] Among earlier attempts toward direct attachment of PS I to Au substrates for photovoltaic applications, chemical platinization of PS I to facilitate PS I welding to Au via PS I−Pt−Au bonding[13] affinity is noteworthy. However, the fact that the mechanism for such chemical "welding" is not very well understood raises questions about the repeatability and uniformity of deposition in these more complex approaches. Other immobilization approaches have utilized bioengineered polyhistidine tags that can self-assemble onto a thiol-coupled Ni-NTA complex on Au surface. However, this system results in a relatively large PS I−Au distance with an inverted electron transport vector facing inward toward the gold,[6] thereby making the electron transport process more challenging, added to the fact that the relatively low affinity of a His-tag for the NTA makes it difficult to achieve a uniform surface coverage.

*Corresponding author. Bamin Khomami; E-mail: bkhomami@utk.edu.

(1) Nelson, N.; Yocum, C. F. *Annu. Rev. Plant Biol.* **2006**, *57*, 521–565.
(2) Nelson, N. *J. Nanosci. Nanotechnol.* **2009**, *9*(3), 1709–1713.
(3) Bruce, B. D.; Malkin, R. *J. Biol. Chem.* **1988**, *263*(15), 7302–7308.
(4) Jordan, P.; Fromme, P.; Witt, H. T.; Klukas, O.; Saenger, W.; Krauss, N. *Nature* **2001**, *411*(6840), 909–917.
(5) Ko, B. S.; Babcock, B.; Jennings, G. K.; Tilden, S. G.; Peterson, R. R.; Cliffel, D.; Greenbaum, E. *Langmuir* **2004**, *20*(10), 4033–4038.
(6) Das, R.; Kiley, P. J.; Segal, M.; Norville, J.; Yu, A. A.; Wang, L. Y.; Trammell, S. A.; Reddick, L. E.; Kumar, R.; Stellacci, F.; Lebedev, N.; Schnur, J.; Bruce, B. D.; Zhang, S. G.; Baldo, M. *Nano Lett.* **2004**, *4*(6), 1079–1083.
(7) Carmeli, I.; Frolov, L.; Carmeli, C.; Richter, S. *J. Am. Chem. Soc.* **2007**, *129*, 12352–12353.
(8) Frolov, L.; Rosenwaks, Y.; Carmeli, C.; Carmeli, I. *Adv. Mater.* **2005**, *17*(20), 2434–2437.
(9) Maly, J.; Krejci, J.; Ilie, M.; Jakubka, L.; Masojidek, J.; Pilloton, R.; Sameh, K.; Steffan, P.; Stryhal, Z.; Sugiura, M. *Anal. Bioanal. Chem.* **2005**, *381*(8), 1558–1567.
(10) Kincaid, H. A.; Niedringhaus, T.; Ciobanu, M.; Cliffel, D. E.; Jennings, G. K. *Langmuir* **2006**, *22*(19), 8114–8120.
(11) Ciobanu, M.; Kincaid, H. A.; Lo, V.; Dukes, A. D.; Jennings, G. K.; Cliffel, D. E. *J. Electroanal. Chem.* **2007**, *599*(1), 72–78.
(12) Lee, I.; Lee, J. W.; Greenbaum, E. *Phys. Rev. Lett.* **1997**, *79*(17), 3294–3297.
(13) Lee, J. W.; Lee, I.; Greenbaum, E. *Biosens. Bioelectron.* **1996**, *11*(4), 375–387.

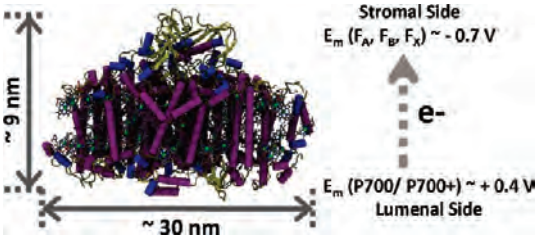

Figure 1. Schematic of Photosystem I (PS I) showing dimensions and directionality of photoinduced electron transfer.

Also, this system was not utilizing the trimeric PS I complex from cyanobacteria, which may behave differently than monomeric PS I complexes from higher plants.[14] The demonstration of extreme thermostability of PS I isolated from TE makes this complex of great interest for future applied work.[15,16]

Although the aforementioned studies have provided valuable information regarding PS I interfaces with various organic/inorganic substrates, none of them provide conclusive evidence of a uniform monolayer formation on the substrate. Hence, researchers interested in utilizing PS I/SAM/Au systems for biosensors, biohybrid photovoltaic applications, or bioelectronic devices are armed with minimal guidance regarding the formation of PS I monolayers on substrates of interest. Experimental results from the present study indicate that PS I solution-phase concentration and deposition technique control protein−protein and protein−surface interactions during PS I adsorption on to SAM/Au substrates. Hence, optimal experimental conditions that lead to uniform surface morphology of PS I with various deposition techniques have been identified.

Materials and Methods

A. Chemicals and Materials Used. Commercial gold-coated silicon wafers with titanium adhesion layer (Au thickness ~100 nm) were purchased from Platypus Technologies. Dibasic (Na_2HPO_4) and monobasic (NaH_2PO_4) sodium phosphate with >99% assay were purchased from Fisher Scientific to prepare the aqueous buffer solutions of 200 mM Na phosphate with pH = 7.0. Concentrated hydrochloric (HCl with ~38% assay) and nitric (HNO_3 with ~69.2% assay) acids purchased from Fisher Scientific were used to prepare fresh Aqua Regia. Ethanol (>99% purity) purchased from Decon Laboratory Inc. was used as the organic solvent to prepare thiol solutions and isopropanol (electronic grade with >99% purity) from Acros Organic was used as the organic cleaning reagent for all the substrates. Concentrated 11-mercapto-1-undecanol (5 mM in ethanol with 97% purity), lysozyme (~95% protein assay), and calcium chloride ($CaCl_2$, 99%) were purchased from Sigma-Aldrich. Magnesium chloride ($MgCl_2$ crystals, >99%) and 2-(4-morpholino)-ethane sulfonic acid (MES with >98% purity) were obtained from Fisher Scientific. Sodium bromide (NaBr) and magnesium sulfate ($MgSO_4$, 99% purity) were from Mallinckrodt. Dodecyl maltoside (DM) was purchased from Glycon Biochemicals GmbH (Luckenwalde, DE), whereas Triton X-100 (TX-100, 10% w/v aqueous solution) was obtained from Anatrace. Sorbitol (D-Sorbitol, 97%) was obtained from Acros Chemicals.

B. Methods. *1. Growth of T. elongatus and Preparation of Photosystem I.* The thermophilic cyanobacterium *Thermosynechococcus elongatus* BP-1 was grown in 2 L airlift fermenters (Bethesda Research Laboratories, Bethesda, MD) in NTA media.[17] The temperature was held at 56 °C with continuous illumination by fluorescent lights. The light level was increased as the cultures approached higher densities to a maximum of 50 μE/m^2/s. Cells were collected during late log phase by centrifugation for 10 min at 7000 *g* and washed once in wash buffer, 20 mM MES pH 6.5, 5 mM $MgCl_2$, and 5 mM $CaCl_2$ before storage at −20 °C until use for PS I preparation. Frozen cells were resuspended in 20 mM MES pH 6.5, 5 mM $MgCl_2$, 5 mM $CaCl_2$, and 500 mM sorbitol. The resuspended cells were adjusted to a *Chl a* content of 1 mg/mL[17] and homogenized using a Dounce homogenizer. Lysozyme was added to 0.2% (w/v) and the mixture was incubated for 2 h at 37 °C with shaking. The resulting mixture was centrifuged as before, and the supernatant was discarded. The pellet was resuspended in the wash buffer. Again, the volume was adjusted so that the *Chl a* concentration was 1 mg/mL; the mixture was then lysed in a French press at 20 000 psi (*g*) twice. The highly fluorescent lysate was centrifuged at 20 000 rpm in a Sorvall centrifuge with a SS-34 rotor for 20 min, and the supernatant was discarded. The crude membrane fragments collected in the pellet were washed once with a wash buffer containing 3 M NaBr, then twice in the initial wash buffer. The final washed membrane fragments were adjusted to a *Chl a* concentration of 1 mg/mL, and dodecyl maltoside (DM) was added to a final concentration of 0.6% w/v and the mixture was incubated for 20 min at 20 °C in darkness with gentle stirring. The insoluble material was removed from the solubilized membrane mixture by centrifugation in the SS-34 at 20 000 rpm (~50 000 *g*) for 30 min. The supernatant was separated immediately from the pellet and then loaded onto 10−30% sucrose gradients with 60% cushion; all solutions in the gradient also contained 20 mM MES and 0.03% DM. Density gradient centrifugation was performed at 24 000 rpm in an SW28 rotor at 10 °C for 16 h. The lowest green band contained the trimeric PS I complex; these bands were collected and pooled using a large syringe. Pooled PS I samples were slowly diluted 5-fold by addition of MES pH 6.5 with 0.03% DM (w/v), and then loaded onto a POROS 20HQ (Applied Biosystems) anion exchange column and eluted with $MgSO_4$ in a minimal volume. Finally, the $MgSO_4$ was removed by dialyzing against 20 mM MES pH 6.5, 500 μM $CaCl_2$, 500 μM $MgCl_2$, and 0.03% DM, and based on spectrophotometer measured chlorophyll concentrations, PS I concentration in the buffer solution was estimated to be around $C_B = 1.42 \times 10^{-5}$ mol/L. PS I were frozen and stored in aliquots of 1.5 mL at −80 °C until used.

2. Preparation of Alkanethiolate SAM/Au Substrates. Commercial Au coated Si wafers were dipped in Aqua Regia (HNO_3 and HCl acids in volumetric ratio of 1:3, respectively). In turn, these freshly etched Au substrates (Au thickness ~60−70 nm) were immersed in 1 mM 11-mercapto-1-undecanol (~24−36 h) at room temperature in a chamber filled with inert dry N_2. Thiolated Au substrates were washed in isopropanol, deionized water, and finally dried in dry N_2 stream. Monolayer formation was confirmed by measuring the thiol thickness on Au substrates at multiple spots using an ellipsometer. For the alkanethiol with C11 chain length used in this study, the thicknesses were measured to be around 0.9−1.1 nm.

3. Preparation of PS I/SAM/Au Substrates. The alkanethiolate SAM/Au substrates were immersed in different concentrations of PS I prepared by diluting concentrated PS I samples in 200 mM Na phosphate aqueous buffer solutions with pH = 7.0 and balanced with 0.02% TX-100 as the detergent for bulk suspension of PS I. Surface immobilization for gravity-driven deposition on thiolated Au substrates was carried out for 5 min.

Electric field assisted depositions were carried out by using an in-house parallel plate electrode assembly (details shown in Figure 2) connected to a stable constant voltage power source

(14) Amunts, A.; Toporik, H.; Borovikova, A.; Nelson, N. *J. Biol. Chem.* **2010**, *285*(5), 3478–3486.
(15) Matsumoto, K.; Vaughn, M.; Bruce, B. D.; Koutsopoulos, S.; Zhang, S. G. *J. Phys. Chem. B* **2009**, *113*(1), 75–83.
(16) Iwuchukwu, I. J.; Vaughn, M.; Myers, N.; O'Neill, H.; Frymier, P.; Bruce, B. D. *Nat. Nanotechnol.* **2010**, *5*(1), 73–79.
(17) Talling, J. F.; Driver, D. Some problems in the estimation of chlorophyll a in phytoplankton In *Primary productivity measurement, marine and freshwater, Washington, DC, 1963*; Doty, M., (Ed.; U.S. Atomic Energy Commission: Washington, DC, **1963**.

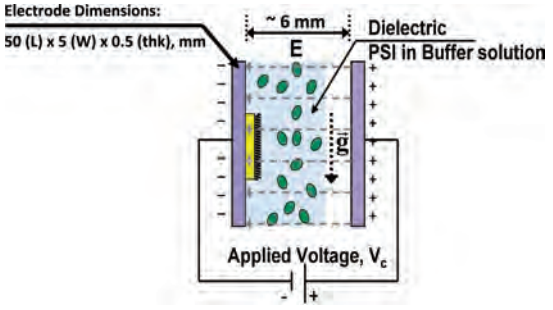

Figure 2. Schematic showing the arrangement and dimensions of the in-house parallel plate electrode assembly used for dielectrophoresis assembly of Photosystem I (PS I) on SAM/Au substrates.

meter (make, Keithley; model, 2400) to generate the desired electric field across the aqueous buffer solution of PS I. Due to lack of surface charge distribution data for the protein complexes, SAM/Au substrates were mounted on both positive (cathode) and negative (anode) plates, and preliminary experiments were performed with dilute PS I suspensions (400 times diluted case) as the electrolyte. A voltage of 2.25 V was applied for 5 min across the PS I suspension. The substrate mounted on the cathode was found to be completely devoid of any PS I, whereas the substrate on the anode showed uniform but sparse deposition of PS I protein complexes. The significant deposition on the anodic substrate also substantiates a net positive surface charge on the protein for the particular ionic strength of the buffer used, which is in agreement with earlier works.[12,18] Thus, for the electric field-assisted deposition experiments, SAM/Au substrates were always mounted on the anodic plate, and a constant voltage of 2.25 V was applied across the electrodes which generated a current of around 0.4−0.5 mA for the specific arrangements of our electrodes as shown in Figure 2. The low voltage also ensured optimal current density that would not denature the proteins or damage the substrate. PS I immobilized SAM/Au substrates were finally washed in buffer solution and deionized water and dried under N_2 stream.

4. Ellipsometry. All thicknesses for alkanethiol monolayer and protein layers on the SAM/Au substrates were measured using a Gaertner Scientific Corp. make Stokes ellipsometer (model L116S F300) operating with a laser wavelength of 632.8 nm at an angle of incidence of 70° and a polarizer angle of 45.54°. All thicknesses estimated from the ellipsometer data were derived using a two-layer model. The alkanethiol monolayer was measured to be around 0.9−1.1 nm using a refractive index value of 1.33 for 11-mercapto-1-undecanol layers.[19] The PS I layer thicknesses were measured assuming thiol monolayer thickness to be ~0.9 nm and the refractive index of PS I to be around 1.45, which corresponds to the most commonly found refractive indices of typical proteins.[20,21] The mean thicknesses and the corresponding uncertainties at a 95% confidence interval were determined from the standard deviations obtained by making measurements at 10 different spots on each of the samples of the PS I/SAM/Au substrates.

5. Atomic Force Microscopy (*AFM*). All surface topography images were collected on an Asylum Research Inc. make atomic force microscope (AFM, model MFP-3D-BIO) in the tapping mode. All topographical images were recorded using a silicon tip compatible with softer biological materials (make, Olympus; model AC240TS) having a force constant of 2 N/m and a resonant frequency of 70 kHz.

6. Dynamic Light Scattering (*DLS*). Dynamic light scattering (Zetasizer, Malvern Instruments, Worcestershire, UK) operating with a laser wavelength of 632.8 nm was used to measure the size distribution of PS I in solution. In addition, to gain insight into the aggregation dynamics of PS I solutions, real-time DLS characterization of PS I suspensions under the influence of externally applied electric fields were performed by mounting the in-house parallel plate electrode assembly inside the DLS setup. All size distributions obtained from DLS data were collected using 178° backward scattering and averaged over six experimental runs each of which was averaged over 12−13 time correlograms fitted by the in-built software of the Zetasizer. All sizes reported in the size distribution data are the equivalent spherical hydrodynamic radii as estimated from Stokes−Einstein relation wherein the effective thermophysical properties of 200 mM Na phosphate aqueous buffer solutions with pH = 7.0 were taken into consideration.

Results and Discussion

A. Gravity-Driven Self-Assembly Technique. Surface topography AFM images (Figure 3A−E) of PS I deposition from higher concentration solutions (Figure 3A−C) indicate large columnar clusters on SAM/Au substrates that dissipate into more uniform layers at lower concentrations (Figure 3D,E). Corresponding ellipsometry data in Figure 3F depicting mean PS I thicknesses on SAM/Au substrates for different concentrations (marked a−e) also support this observation. At the highest concentration case (a), a mean thickness of 63.2 ± 3.3 nm is observed. As the PS I concentration is reduced, the film thickness also decreases to 35.4 ± 5.4 nm and 29.8 ± 5 nm (b and c, respectively). At lower concentration cases (d and e), much lower thicknesses of 14.2 ± 0.5 nm and 12.7 ± 1.3 nm are observed. Large error bars in the thicknesses for depositions from high PS I concentration cases of 2.9×10^{-4} mM (50×), 7.2×10^{-5} mM (200×), and 3.6×10^{-5} mM (400×) (a, b, and c in Figure 3F) indicate wide variations in the columnar structures across the surfaces as compared to the relatively homogeneous PS I distributions indicated by the smaller error bars for lower concentration cases (d and e in Figure 3F). The bracketed values next to the concentrations reported indicate the amount by which the concentrated PS I samples are diluted, and X is the dilution factor with respect to the base concentration of 1.427×10^{-5} mol/L. These images and the corresponding film thickness measurements clearly indicate the complexity of the morphologies obtained from gravity-driven deposition of PS I on SAM/Au substrates.

One of the challenges of creating a uniform PS I monolayer with this deposition technique lies in the formation of large PS I aggregates in the solution, which in turn results in columnar clusters of deposited proteins. To clearly demonstrate the interrelation between aggregate formation in the bulk and the surface morphology of PS I thin films, DLS experiments have been used to approximate particle size distribution (PSD) for the representative PS I solution concentrations of 7.2×10^{-5} mM (200×), 3.6×10^{-5} mM (400×), and 1.8×10^{-5} mM (800×). Figure 4 depicts our principal findings, namely, at high bulk protein concentration of 7.2×10^{-5} mM (i.e., 200× dilutions) large structures (> 2000 nm) are observed. As the PS I solution concentration is reduced to 3.6×10^{-5} mM and 1.8×10^{-5} mM (i.e., 400× and 800× dilution, respectively), the cluster sizes clearly shift to smaller-sized bins (< 1000 nm) and secondary peaks of smaller cluster sizes (< 400 nm and even, 100 nm) emerge. Hence aggregate formation is clearly suppressed due to reduction of PS I solution concentration in the bulk phase.

These observations also support our surface film morphologies, namely, the formation of large columnar structures at high

(18) Gross, E. L. *Photosynth. Res.* **1993**, *37*(2), 103–116.
(19) Ehler, T. T.; Malmberg, N.; Noe, L. J. *J. Phys. Chem. B* **1997**, *101*(8), 1268–1272.
(20) Tengvall, P.; Lundström, I.; Liedberg, B. *Biomaterials* **1998**, *19*(4−5), 407–422.
(21) Vörös, J. *Biophys. J.* **2004**, *87*(1), 553–561.

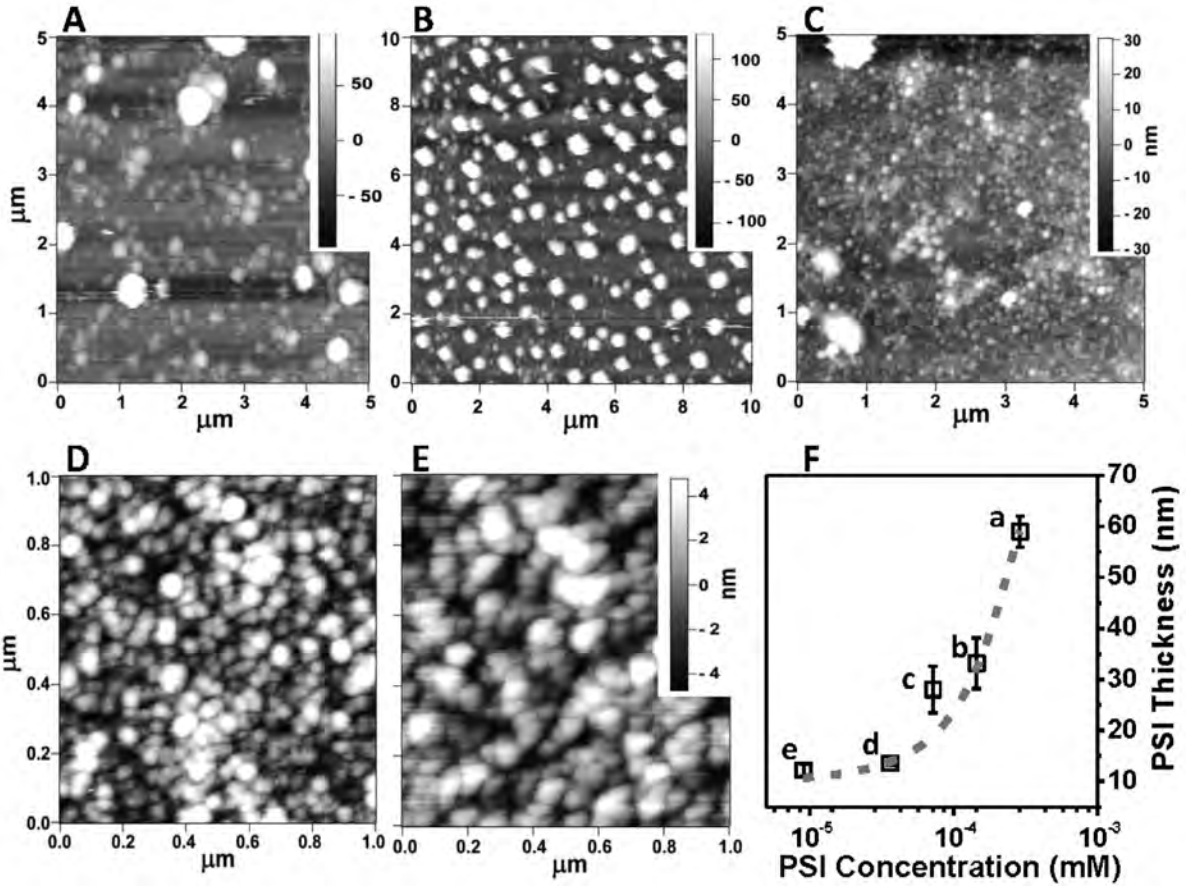

Figure 3. Surface topographical AFM images of PS I/SAM/Au substrates prepared from different PS I concentrations of (A) 2.9×10^{-4} mM (50×); (B) 7.2×10^{-5} mM (200×); (C) 3.6×10^{-5} mM (400×); (D) 1.8×10^{-5} mM (800×); and (E) 9.1×10^{-6} mM (1600×) (bracketed values indicate dilutions, X being the dilution factor) obtained by diluting base concentration of $C_B = 1.427 \times 10^{-5}$ mol/L with aqueous buffer solutions (as described in the article). (F) Elipsometry data indicating mean thicknesses (nm) of PS I adsorbed onto SAM/Au substrates corresponding to the AFM iamges (A−E) (indicated as a−e on the figure). Error bars indicate uncertainties in data for multiple readings collected. The gray dashed line indicates the best curve fitted to the experimental data. All AFM images collected with a tip of spring constant 2 N/m in tapping mode.

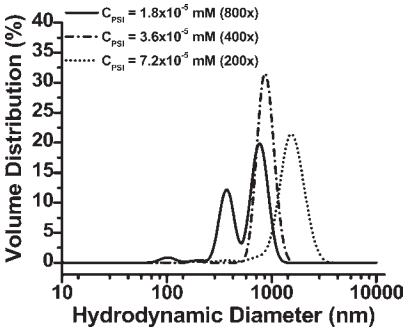

Figure 4. Representative particle size distribution data from dynamic light scattering (DLS) measurements of PS I suspensions with 7.2×10^{-5} mM (200×), 3.6×10^{-5} mM (400×), and 1.8×10^{-5} mM (800×) concentrations in 200 mM Na phosphate buffer solutions (0.02% w/v TX-100 as detergent).

PS I concentrations. It should be noted that the agglomerates have columnar structures due to preferential top−bottom alignment of PS I that results from steric hindrance effectively caused by the dipole screening as a result of the attachment of detergent molecules to the protein rim.[22] As the dilution is increased, protein−protein interactions are weakened thereby preventing agglomeration and, in turn, resulting in relatively uniform layers of PS I on the substrate. However, in the dilution range studied PS I clustering could not be completely eliminated. In fact, we observe a minimum cluster size beyond which the formation of PS I aggregates cannot be thwarted any further as indicated by the DLS data in Figure 4. Hence, this approach of decreasing the PS I layer thicknesses on the substrates through systematic solution-phase dilution might not necessarily be an efficient way to generate a uniform monolayer of PS I on the substrate.

B. Electric Field Assisted Directed-Assembly Technique. To overcome solution-phase aggregation, a directed assembly technique using electric field of various strengths is employed. The technique essentially makes use of the interactions of the electric field with the inherent dipole moment of the PS I molecules in the direction perpendicular to the central axes of the aggregated columnar structures. Encouraged by the preliminary results indicating a net positive charge of PS I,[12] we designed a series of experiments using various incubation times and PS I concentrations to monitor protein deposition under external electric fields applied to deaggregate the proteins in solution phase as well as driving the deposition.

The mechanistic role of electric field in PS I deaggregation process in solution phase is elucidated with the aid of PSDs measured using in situ DLS experiments on a fully agglomerated system of PS I suspension in buffer solutions under various

(22) Muh, F.; Zouni, A. *Biochim. Biophys. Acta* **2008**, *1778*(10), 2298–2307.

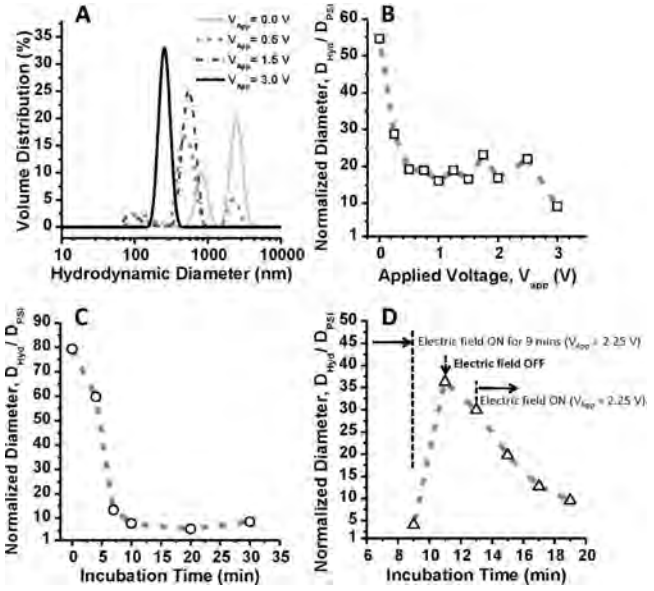

Figure 5. (A) Representative particle size distributions (PSD) of PS I aggregate clusters in aqueous buffer solutions (200 mM Na phosphate buffer with 0.02% w/v TX-100 as detergent) as measured with in situ DLS experiments under applied voltages of V_{App} = 0.0, 0.5, 1.5, and 3.0 V. (B) Corresponding variation of volume-averaged hydrodynamic diameter (D_{Hyd}, nm) as estimated from real-time PSDs and normalized by equivalent spherical diameter of single PS I trimer ($D_{PS\ I}$ ~28 nm) over a complete range of V_{App} = 0−3 V. (C) Normalized volume-averaged hydrodynamic diameter ($D_{Hyd}/D_{PS\ I}$) as estimated from real-time DLS-based PSDs collected over PS I suspensions exposed to applied electric field with V_{App} = 2.25 V for different time periods. (D) Effect of the presence or absence of applied electric field on the normalized volume-averaged hydrodynamic diameter ($D_{Hyd}/D_{PS\ I}$) as monitored in real time.

applied voltages (V_{App}). PS I concentration of 7.2×10^{-5} mM, i.e., 200× dilution along with 0.02% w/v TX-100 as detergent was used for this study. Typical results (V_{App} = 0, 0.5, 1.5, and 2.5 V) of the scattering studies are shown in Figure 5A. Large clusters of PS I aggregates (peak diameters ≥1000 nm) formed in the absence of an electric field (V_{App} = 0 V) break down to form smaller clusters with increasing V_{App} as suggested by the suppression of the 3000 nm peak accompanied by a corresponding emergence of smaller peak (~500 nm) at V_{App} = 0.5 V. The smaller-sized clusters increase in volume as V_{App} is further increased to 1 V, and eventually at V_{App} = 3 V, the bimodal distributions completely shift into a single peak at 200−300 nm. This systematic breakdown of PS I aggregates is clearly observed in Figure 5B showing the variation of volume-averaged hydrodynamic diameters, D_{Hyd} (estimated from similar PSDs collected over a wide range of V_{App}) normalized by equivalent spherical diameter of single PS I trimer, $D_{PS\ I}$ (~28 nm as estimated from shape factors for oblate spheroids with dimensions given in Figure 1) as a function of increasing applied voltages. This phenomenon is attributed to the applied electric field effectively interacting with the intrinsic dipole moment of PS I to create a force field that eventually overcomes the PS I−PS I bonding in the aggregates, thereby resulting in smaller clusters of PS I being fragmented and released from the aggregates that get directed onto the substrate under the applied field. In this process, individual PS I trimers with higher dielectrophoretic mobility will have a higher propensity to quickly migrate to the electrode surface, thereby resulting in a relatively uniform PS I layer on the substrate. It should be noted that the PSDs obtained here from DLS experiments were collected for voltages applied across the PS I suspension in buffer for 2−4 min.

In order to effectively ascertain the dynamics of the protein dipole interactions with the applied voltage, PSDs were further collected from real-time DLS experiments on PS I suspensions being exposed to V_{App} = 2.25 V (to minimize protein damage possibly due to high current density at higher voltages applied for longer times) for different time intervals. The results, as presented in Figure 5C, immediately indicate that the normalized volume-averaged hydrodynamic diameter ($D_{Hyd}/D_{PS\ I}$) of PS I clusters, as estimated from the PSDs, systematically decreases as their exposure time to the electric field is increased from 0 to 30 min. Interestingly, beyond 10−15 min of exposure to the field, PS I aggregate sizes are barely 4−5 times that of a single PS I trimer. This again reiterates the aforementioned phenomenon of fragmentation of the PS I aggregates wherein the trimers (due to their highest mobility) quickly migrate to the electrode surface, thereby allowing the scattering data to only track the fragmented PS I clusters left in the bulk solution. To further validate the aforementioned mechanism of PS I deaggregation under electric field, PS I cluster sizes are also monitored by carrying out real-time DLS measurements on PS I suspension initially exposed to the electric field (V_{App} = 2.25 V) for 9 min subsequently followed by monitoring the cluster sizes in alternating absence and presence of an applied electric field. The results reveal that initially under the applied field $D_{Hyd}/D_{PS\ I}$ depicts relatively smaller clusters that quickly increase in size when the applied voltage is switched off (Figure 5D). Upon reapplication of the electric field, the cluster sizes decline steadily, thereby indicating a systematic deaggregation of the PS I clusters.

Furthermore, the effect of PS I deaggregation induced by the external electric field on the effective surface topography of PS I deposited on SAM/Au substrates was systematically studied using AFM and ellipsometry characterizations on electric field assisted assembly carried out under various incubation time and PS I concentrations. In the first set of experiments, the effect of varying PS I concentrations in aqueous buffer solutions on the deposition dynamics of electric field assisted assembly of PS I is studied. Aqueous buffer suspensions with PS I concentrations of 1.8×10^{-5} mM (800×), 7.2×10^{-5} mM (200×), 2.8×10^{-4}mM (50×), 5.4×10^{-4} mM (25×), and 1.4×10^{-3} mM (10×) are subjected to an applied voltage of 2.25 V. The incubation time is fixed at 15 min based on our earlier experiments revealing that, beyond this exposure time to the electric field, PS I aggregates undergo maximum deaggregation thereby leading to an increased release of PS I trimeric complexes migrating to the electrodes. In this case, AFM topographical images show minimal PS I deposition for the 1.8×10^{-5} mM (800×) case (Figure 6A). The small circular spots of diameter ~30−40 nm represent the PS I trimers, thereby indicating that most of them undergo surface attachment on their luminal (bottom) side (see Figure 1). The density of deposited proteins, although sparse, increases as the PS I concentration is increased to 7.2×10^{-5} mM (200×) and 2.8×10^{-4} mM (50×) (Figure 6B,C). Specifically, at PS I concentrations of 5.4×10^{-4} mM (25×) and 1.4×10^{-3} mM (10×), the deposition patterns indicate denser and, yet, uniform layers of PS I (Figure 6D,E). Added to this, the ellipsometry data in Figure 6F reveal thicknesses that support AFM observations for the different concentration cases (represented as a, b, c, d, and e) by indicating a negligible film thickness of 0.03 ± 0.07 nm for case a (i.e., 0.3% surface coverage, based on the fact that PS I sitting on its luminal side will have an effective maximum height of 9 nm). This barely increases to 1.2 ± 0.2 nm (15% surface coverage) for case b. On the other hand, the PS I deposition thicknesses

 DOI: 10.1021/la102832x E

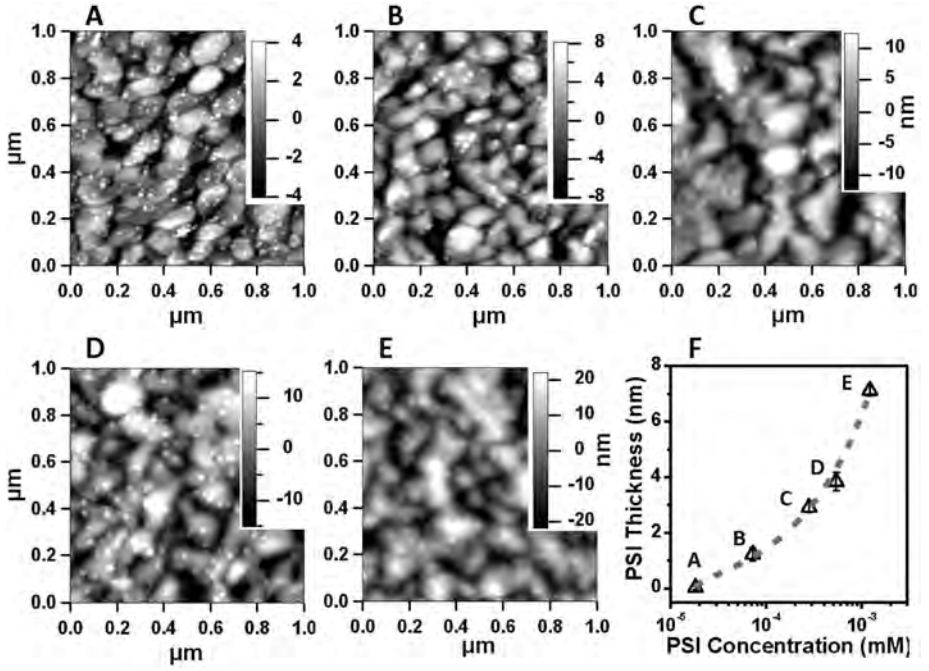

Figure 6. Surface topographical AFM images of PS I/SAM/Au substrates prepared using electric field assisted directed assembly from different PS I concentrations of (A) 1.8×10^{-5} mM (800×), (B) 7.2×10^{-5} mM (200×), (C) 2.8×10^{-4} mM (50×), (D) 5.4×10^{-4} mM (25×), and (E) 1.4×10^{-3} mM (10×) in aqueous buffer solutions for a fixed incubation time of 15 min (as described in the article). (F) Elipsometry data indicating mean thicknesses (nm) of PS I adsorbed onto SAM/Au substrates corresponding to the AFM images (A−E) (indicated as a−e in the figure). Error bars indicate uncertainties in data for multiple readings collected. The gray dashed line indicates the best curve fitted to the experimental data with $R^2 = 0.993$ (discussed in detail in the article). All AFM images collected with a tip of spring constant 2 N/m in tapping mode.

gradually increase to 2.9 ± 0.2 nm, 3.8 ± 0.3 nm, and, finally, 7.1 ± 0.2 nm corresponding to 32%, 43%, and 79% surface coverage, respectively (cases c, d, and e, respectively).

In the second set of experiments, a voltage of 2.25 V, applied across the electrodes for incubation time periods of 2, 3, 5, 15, and 30 min, is used to deposit PS I onto the SAM/Au substrate. Here, a fixed and relatively high PS I concentration of 1.43×10^{-3} mM (i.e., 10× dilutions on the base concentration) is specifically chosen to analyze the deposition pattern at an extremely high PS I concentration. AFM topographical images of the substrates in each of the cases reveal that a sparse, yet uniform, distribution of individual PS I trimers devoid of any aggregation (as seen in Figure 7A and B where the small circular spots of sizes ∼30−40 nm represent the PS I trimers). However, increasing the incubation time to 5 min increases the PS I deposition (Figure 7C), which eventually turns into a dense and yet uniform layer of PS I (Figure 7D,E) as the incubation time is further increased to 15 and 30 min, respectively. It is noted here that Figure 7C,D,E reveals the depositions to be dense but devoid of any columnar structures or aggregation, similar to the deposition patterns obtained earlier for the higher-concentration cases (see Figure 6C,D,E). This also corroborated by the thickness measurements from ellipsometry experiments (represented as cases a, b, c, d, and e in Figure 7F). A thin layer of PS I with an effective thickness of 1.0 ± 0.3 nm and 2.4 ± 0.2 nm is formed for the incubation times of 2 and 3 min (a and b), which translates to a surface coverage of about 11% and 27%, respectively. On the other hand, increased incubation times of 5, 15, and 30 min lead to deposition thicknesses 4.0 ± 0.7 nm, 7.1 ± 0.2 nm, and 7.5 ± 0.6 nm (c, d, and e, respectively), which corresponded to much higher surface coverage of ∼45%, 79%, and 83%, respectively. In both cases presented above, the maximum surface coverage of about 79−83% is consistent with the packing density of oblate spheroid (or circular on 2D space) particles with 9 nm height being, at the most, 0.9−0.91 for an optimal hexagonal packing on the surfaces. These data are consistent with the earlier solution-phase DLS measurements indicating significant fragmentation of the PS I aggregates only beyond 10 min of incubation time under an applied electric field of $V_{App} = 2.25$. Also, the variability in the measured thicknesses, as indicated by the error bars accounting for multiple data collections, does not indicate the same large variability in film thicknesses as observed earlier in the ellipsometry data for the gravity-driven cases, thereby implying that this deposition process is more uniform and reproducible.

These results suggest the aforementioned phenomenon to be a reversible process in which the imposed electric field during assisted deposition of PS I is able to break down the PS I columnar aggregates into smaller clusters in solution phase, of which the individual PS I trimeric complexes, with higher mobility, are quickly driven toward the desired surfaces. On the other hand, in the absence of the field, PS I trimers undergo rapid aggregation and quickly assemble back into their aggregated clusters with PS I−PS I homotypic interactions that are difficult to disrupt. Also, PS I depositions with various incubation times and concentrations in electric field assisted assembly indicate a controlled process that starts with sparse and eventually ends in a uniform, homogeneous monolayer, thereby allowing excellent control over PS I adsorption onto SAM/Au substrates. This conclusion is based on our observations from both AFM studies and ellipsometric data. First, the error bars in Figures 6F and 7F indicate relatively insignificant variations in the uncertainties of the thicknesses measured by ellipsometry, thereby establishing the homogeneity of the PS I depositions. Second, a sideways attachment, or stacking arrangement of PS I on the surfaces, would have resulted in the overall topography indicating an average layer thickness of >10 nm (and $\leq 30-40$ nm for a

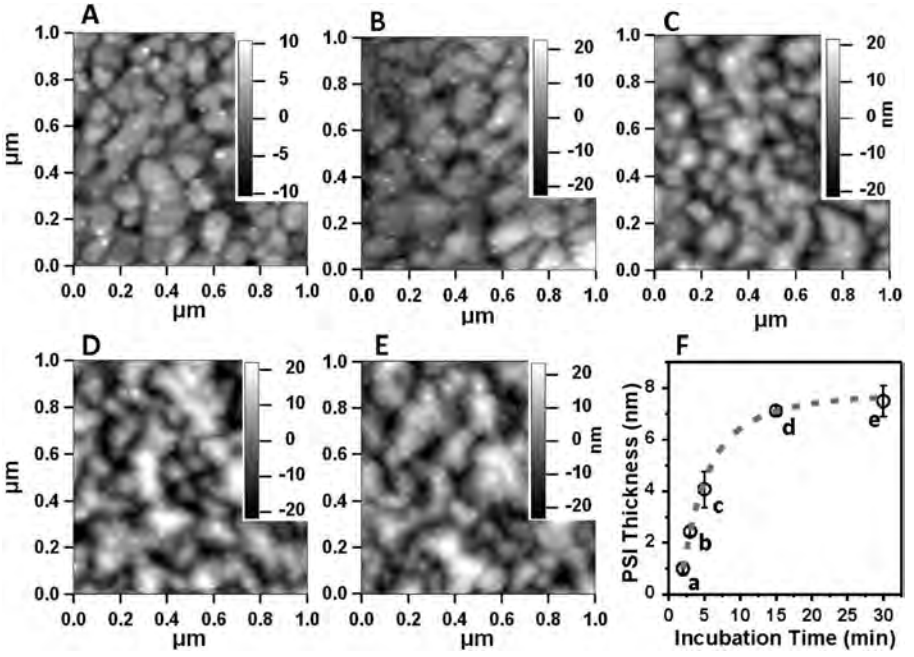

Figure 7. Surface topographical AFM images of PS I/SAM/Au substrates prepared using electric field assisted directed assembly for different incubation times of (A) 2 min; (B) 3 min; (C) 5 min; (D) 15 min; and (E) 30 min from PS I concentration of 1.43×10^{-3} mM (10× dilutions) in aqueous buffer solutions (as described in the article). (F) Elipsometry data indicating mean thicknesses (nm) of PS I adsorbed onto SAM/Au substrates corresponding to the AFM images (A−E) (indicated as a−e in the figure). Error bars indicate uncertainties in data for multiple readings collected. The gray dashed line indicates the best curve fitted to the experimental data with $R^2 = 0.997$ (discussed in detail in the article). All AFM images collected with a tip of spring constant 2 N/m in tapping mode.

sparse PS I distribution), contrary to the average thicknesses of ≤9 nm as observed from ellipsometry measurements of all the cases studied here (see Figures 6F and 7F) along with the effective circular shapes of 30−40 nm diameters as expected for PS I trimers (see AFM images in Figures 5 and 6). These observations clearly point toward a significant number of PS I's lying on their broader, circular base without being stacked on top of each other thereby forming a uniform, homogeneous monolayer of PS I on SAM/Au substrates.

Conclusion

The present studies on PS I deposition dynamics for simple gravity-driven self-assembly and electric field assisted directed assembly techniques indicate that, in the absence of an external field, PS I suspension in buffer suffers from bulk aggregation, which becomes predominant in suspensions with higher PS I concentrations due to heightened protein−protein interactions. This coupled with specific steric attachments favors the formation of columnar structures which, in turn, deposit intact onto the substrate. In lower-concentration cases, less frequent protein−protein interactions reduce the tendency toward significant aggregation, thereby enabling smaller PS I clusters to generate relatively uniform PS I layers on the substrate. Finally, results from electric field assisted PS I deposition demonstrate that externally imposed electric field is able to effectively break up the columnar aggregates of PS I in buffer solutions, thereby driving individual trimetric PS I complexes to the SAM/Au substrates with a mobility that is commensurate with the applied electric field. This in turn allows a systematic and rapid deposition of PS I monolayers on SAM/Au substrates. In light of translating benchtop experiments to commercial fabrication of PS I based bioelectronic devices or biosensors, the aforementioned results could play a central role in the design of protein deposition systems that enable systematic uniform monolayer formation through directed/field assisted deposition.

Acknowledgment. This work was funded by Sustainable Energy Education and Research Center (SEERC) at UTK to B.D.B. and B.K. This work was also supported by a National Science Foundation (NSF) Nanoscience Interdisciplinary Research Team (NIRT) award to B.D.B. (DBI-0403781). Partial support for D.M. was provided by the Gibson Family Fellowship.